ACS OMEGA

http://pubs.acs.org/journal/acsodf

Article

Human Microglia Extracellular Vesicles Derived from Different Microglia Cell Lines: Similarities and Differences

Lorenzo Ceccarelli, Laura Marchetti,* Milena Rizzo, Aldo Moscardini, Valentina Cappello, Eleonora Da Pozzo, Miriam Romano, Chiara Giacomelli,* Paolo Bergese, and Claudia Martini

Cite This: *ACS Omega* 2022, 7, 23127−23137

Read Online

ACCESS | Metrics & More | Article Recommendations | Supporting Information

ABSTRACT: Microglial cells are a component of the innate immune system in the brain that support cell-to-cell communication via secreted molecules and extracellular vesicles (EVs). EVs can be divided into two major populations: large (LEVs) and small (SEVs) EVs, carrying different mediators, such as proteins, lipids, and miRNAs. The microglia EVs cargo crucially reflects the status of parental cells and can lead to both beneficial and detrimental effects in many physiopathological states. Herein, a workflow for the extraction and characterization of SEVs and LEVs from human C20 and HMC3 microglia cell lines derived, respectively, from adult and embryonic microglia is reported. EVs were gathered from the culture media of the two cell lines by sequential ultracentrifugation steps and their biochemical and biophysical properties were analyzed by Western blot, transmission electron microscopy, and dynamic light scattering. Although the C20- and HMC3-derived EVs shared several common features, C20-derived EVs were slightly lower in number and more polydispersed. Interestingly, C20- but not HMC3-SEVs were able to interfere with the proliferation of U87 glioblastoma cells. This correlated with the different relative levels of eight miRNAs involved in neuroinflammation and tumor progression in the C20- and HMC3-derived EVs, which in turn reflected a different basal activation state of the two cell types. Our data fill a gap in the community of microglia EVs, in which the preparations from human cells have been poorly characterized so far. Furthermore, these results shed light on both the differences and similarities of EVs extracted from different human microglia cell models, underlining the need to better characterize the features and biological effects of EVs for therein useful and correct application.

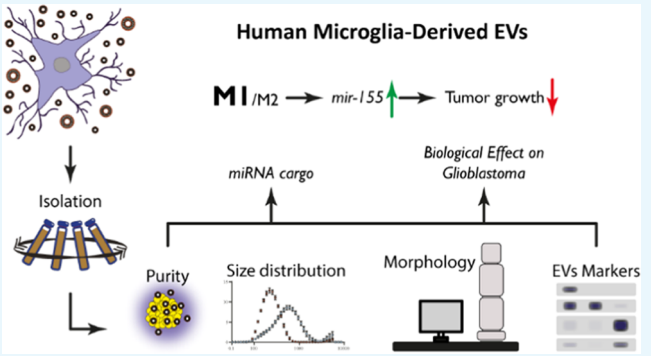

INTRODUCTION

Microglia cells are recognized as the resident macrophages of the central nervous system (CNS), of which they constitute the first defense line. The interest in these cells has rapidly grown in recent years,[1−3] although their effects in physiological and pathological conditions are still controversial.[4−7] For example, microglia play protective but also detrimental roles in several neurological disorders,[8] which often include disease exacerbation via inflammatory response activation.[9] Furthermore, microglia constitute a large percentage of tumor-associated macrophages (TAMs) in glioblastoma, in which, via a plethora of signaling pathways, they modulate opposite trends of tumor progression.[10]

For microglia cells, the secretome is crucial for controlling CNS functioning, and it comprehends secreted factors and released extracellular vesicles (EVs).[11] EVs are particles produced by most cell types in physiological and pathological conditions. Two main types of EVs have been described based on their dimension and biogenesis: large EVs (LEVs, diameter in the 150−800 nm range), generated from outward budding of the plasma membrane, and small EVs (SEVs, diameter in the 30−250 nm range), originating from the fusion of multivesicular bodies with the plasma membrane.[11−14] EVs play a pivotal role in cell-to-cell communication, as well as a shuttle for eliminating unwanted molecules out of the cells, helping the proteasomal and lysosomal systems. The cargo of EVs comprehends proteins, lipids, mRNAs, and miRNAs, and it can drastically change depending on the state of the parental cells.[15,16] Thanks to their long-distance diffusivity in the CNS, microglia-derived EVs can potentially regulate most cell types in the brain, comprising resident, infiltrating cells, and tumoral cells.[1] However, microglial cells have been extensively investigated more as receivers of EVs released from other cell types than as EV producers.[11,17] Importantly, most microglia EVs described so far have been derived from murine (e.g., BV2 and N9 cell lines, or primary

Received: February 9, 2022
Accepted: May 17, 2022
Published: June 28, 2022

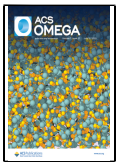

cells) or leech microglia, thus leaving the description of EVs from human microglia cells almost unexplored.[11]

Herein, a rigorous biophysical and biochemical characterization of EVs gathered from two human microglia cell types, namely HMC3[18] and C20[19] cells, is reported. Both cell lines derive from the immortalization of human primary microglia via transduction of the large SV40 T antigen only (HMC3), or the combination of SV40 T antigen with hTERT (C20). Importantly, HCM3 cells derive from human embryonic microglia, while C20 derive from human adult microglia. We demonstrate that most biophysical and biochemical features are shared between HMC3- and C20-EVs. Among the possible EV cargoes, eight miRNAs were investigated and quantified by qPCR, leading to the unexpected observation that most of them are differentially regulated in the two cell lines at basal level. Our work provides new details of human microglia EVs, whose first description has been reported last year[20] in the literature; importantly, the characterization reported here validates the use of these cell lines as an invaluable routine tool for the study of microglial EVs of human origin. However, differences between the miRNA cargoes of two EV types, correlating with their ability to interfere with glioblastoma proliferation, are here highlighted.

MATERIALS AND METHODS

Microglia Cell Culture. All materials for cell culture were purchased from Corning, New York. HMC3 cells (ATCC, Manassas, Virginia) were cultured in MEM (10-009-CV) added with 10% FBS (35-089-CV), 100 U/mL penicillin, and 100 ug/mL streptomycin. C20 cells, originally generated by David Alvarez-Carbonell et al. (Case Western Reserve University)[19] and kindly gifted by Christian H, Wetzel, were cultured in DMEM F12 50/50 (10-092-CV) added with 10% FBS (35-089-CV), 100 U/mL penicillin, 100 ug/mL streptomycin, and 600 ug/mL neomycin. The cells were maintained at 37 °C in a 5% CO_2 incubator. Before EV production, both cell lines were seeded in 152 cm^2 Petri dishes and, once the confluency reached 90−95%, the complete medium was removed, cells were washed once with PBS (D8537-500 ML), and added to the same medium without FBS (Starvation Medium) for many valid reasons, according to MISEV2018 indications, mainly (i) FBS contains high levels of EVs; (ii) serum deprivation increases EV production;[14] (iii) FBS contains high levels of bovine serum albumin (BSA) and other soluble nanoparticles (e.g., lipoproteins) that could be co-isolated with EVs and are considered exogenous contaminants; (iv) microglia grown without serum showed a closer similarity to resting microglia and low levels of activation.[21,22] U87MG cells (CLS Cell Lines Service GmbH, Eppelheim, Germany), a cell line of human glioblastoma, were cultured in RPMI 1640 (15-040-CV) added with 10% FBS, 100 U/mL penicillin, 100 ug/mL streptomycin, and maintained at 37 °C in a 5% CO_2 incubator.

EVs Isolation by Differential Ultracentrifugation. HMC3 and C20 cells were maintained in starvation medium for 16−18 h, the supernatant was collected, and the cells were detached and counted. Cells were maintained in 152 cm^2 Petri dishes with 16 mL of complete medium or 12 mL of starvation medium; the mean amount of cells relative to one 152 cm^2 Petri dish is 12.8×10^6 for C20 cells and 18.1×10^6 for HMC3 cells. Supernatants were centrifuged for 10′ at 4 °C at 1000*g* to remove any cellular debris. Two isolation protocols were used to gather EVs from the cell supernatant: EVs were extracted by single ultracentrifugation at 4 °C at 100,000*g* for 2 h or extracted in two steps, 30′ at 4 °C 16,000*g* to isolate the LEVs, and 2 h at 4 °C 100,000*g* to isolate the SEVs. All EV pellets were washed with an excess of PBS with ions (Sigma cat. D8662), 0.22 μm filtered, and centrifuged again in the same conditions used to extract them. The pellets obtained were suspended in lysis buffer with protease inhibitors or PBS with ions 0.22 μm filtered, depending on the specific use.

Western Blot Analysis of Cells and EVs. Cell pellets were suspended in Ripa Buffer added with Protease inhibitors (Merck KGaA), lysed, and protein content quantified with DC Protein Assay (Bio-Rad).[23] One microgram of total protein content was loaded on a gel for the detection of α-Actinin-4 and 30 μg for each of the other proteins. The EV pellets were suspended and lysed in Ripa Buffer added with the protease inhibitor, and the equivalent quantity of total protein suspension coming from one 100% confluent 152 cm^2 Petri dish was loaded in each lane. All samples were added with Laemmli solution and boiled for 5′ at 95 °C, then an SDS-PAGE was performed in a 4−20% polyacrylamide gel. The following antibodies were used: mouse anti-α-Actinin-4 (sc-390205) 1:500, mouse anti-CD81 (sc-166029) 1:2000, mouse anti-CD63 (sc-5275) 1:250, mouse anti-GM130 (BD Bioscience, 610822) 1:1000, rabbit anti-GAPDH (Sigma, G9545) 1:2500, and anti-rabbit and anti-mouse-HRP (Merk) 1:5000. The band intensity was acquired with ChemiDoc (Bio-Rad) and quantified using Image Lab Software (Bio-Rad). The intensity of the lanes was compared after normalization to the total protein loaded in each lane estimated with the stain-free technology of the Bio-Rad precast gels.

Purity Assessment of C20 and HMC3 EV Subpopulations. The absence of soluble single and aggregated proteins not belonging to EVs (hereafter referred to as exogenous SAPs) was assessed by using the Colorimetric NANoplasmonic assay (CONAN), following the open-access protocol described elsewhere.[24] The purity grade of the 16,000*g* and 100,000*g* EV preparations derived from untreated C20 and HMC3 cells was characterized using a 6 nM solution of gold nanoparticles (AuNPs) with a diameter of 13 nm. The LSPR spectra of three technical replicates for each sample were analyzed by a Perkin-Elmer Ensight Multimode Plate Reader and used to determine the mean relative Aggregation Index (AI).

TEM Analysis. EVs pellets derived from two 152 cm^2 Petri dishes were suspended in 100 μL of PBS with ions, maintained at −80 °C, and thawed only once immediately before analysis. Samples were prepared using a two-step protocol for negative staining as described elsewhere.[25] Briefly, the EV suspension was adsorbed onto the carbon-coated 300 mesh copper grids (Electron Microscope Science, Hatfield, Pennsylvania). The adsorption time varied between 30 and 45 min depending on the sample size and suspension concentration. Then, the grids were washed three times with pure water and stained for 30 s with our homemade *X* solution diluted 1:5 or 1:10 (v/v) in pure water.[26] A dilution of the staining solution is required to reduce EV shrinkage. The grids were then paper-drained and directly analyzed with a ZEISS Libra 120 Plus transmission electron microscope, operating at 120 kV and equipped with an in-column omega filter for energy-filtered imaging. EM micrographs were collected with a 16-bit CCD camera (Zeiss, Oberkichen, Germany) at 20.000−25.000 *X*. The images were finally analyzed with ImageJ software (NIH) for the morphological characterization. They were finally analyzed with ImageJ software (NIH) for the morphological characterization. Each EV diameter was estimated by measuring the

https://doi.org/10.1021/acsomega.2c00816
ACS Omega 2022, 7, 23127−23137

Table 1. List of the Primers Used for This Study

miRNA ID	primers FW
hsa-mir-21-5p	TAGCTTATCAGACTGATGTTGA
hsa-mir-26a-5p	TTCAAGTAATCCAGGATAGGCT
hsa-mir-146a-5p	TGAGAACTGAATTCCATGGGTT
hsa-mir-153-3p	TTGCATAGTCACAAAAGTGATC
hsa-mir-155-5p	TTAATGCTAATCGTGATAGGGGTT
hsa-mir-200b-3p	TAATACTGCCTGGTAATGATGA
hsa-mir-223-3p	TGTCAGTTTGTCAAATACCCCA
hsa-let-7c-3p	CTGTACAACCTTCTAGCTTTCC
IL4_74 bp_55 °C	FW 5′-ACTTTGAACAGCCTCACAGAG-3′
	RV 5′-TTGGAGGCAGCAAAGATGTC-3′
IL6_165 bp_55 °C	FW 5′-TCCTCGACGGCATCTTCA-3′
	RV 5′-TTTTCACCAGGCAAGTCTCCT-3′
TGF-β_218 bp_55 °C	FW 5′-ACTGCAAGTGGACATCAACG-3′
	RV 5′-TGCGGAAGTCAATGTACAGC-3′
TNF-α_101 bp_55 °C	FW 5′-AGGGACCTCTCTCTAATCAGCC-3′
	RV 5′-GCTTGAGGGTTTGCTACAACA-3′
β-actin_254 bp_55 °C	FW 5′-GCACTCTTCCAGCCTTCCTTCC-3′
	RV 5′-GAGCCGCCGATCCACACG-3′
GAPDH_107bp_55 °C	FW 5′-GAGAAGTATGACAACAGCCT-3′
	RV 5′-CCTTCCACGATACCAAAGTT-3′

perimeter (p), approximating it as a circumference and using it to calculate the diameter with the formula $d = p/\pi$.

Dynamic Light Scattering (DLS) Analysis. EVs pellets derived from two 152 cm^2 were suspended in 100 μL of PBS with ions, maintained at −80 °C, and thawed only once immediately before analysis. Dynamic light scattering measurements were performed with a ZetaSizer Nano-ZS90 (Malvern Instruments Inc., Malvern, U.K.). The instrument laser wavelength was 633 nm and, as scattering angle (θ), 90° was chosen. The mean hydrodynamic diameter was calculated from the autocorrelation function of the intensity of scattered light using DTS Nano software (version 1.41, Malvern Instruments Inc., Malvern, U.K.). Briefly, the intensity fluctuations were used to obtain the intensity-weighted distribution (%I_a). %I_a was linked to the size of the macromolecules as shown in eq 1

$$\%I_a = \frac{a^6 N_a \times 100}{N_a a^6 + N_b b^6} \quad (1)$$

where N_a represents the population of molecules with size a and N_b is the population of macromolecules with size b. Summing, the intensity distribution is approximately proportional to the size.[6] Starting from the intensity distribution, a number-weighted distribution (%N_a) can be obtained[27]

$$\%N_a = \frac{N_a \times 100}{N_a + N_b} \quad (2)$$

where only the number of vesicles constituting each population is taken into account. The %N_a distributions obtained for each replica of the SEV sample (2_100K samples) were fitted with a mono-peak Gaussian function

$$y = y0 + A \times \exp(-0.5 \times ((x - x_c)/w) \wedge 2 \quad (3)$$

and the x_c value was used to calculate the average hydrodynamic diameter of the distribution. The mean ± SD of all of the obtained peak values were plotted and analyzed. Fifty microliters of each sample was diluted in PBS to a final volume of 130 μL and measured 5 times.

For a better evaluation of the obtained EV populations, the polydispersity index (PDI) of each population was also calculated, using eq 4. Notably, the ZetaSizer software permits to estimate the vesicle concentration in a sample by knowing the size of a population, its PDI, and its count rate (intensity of the scattered light). The concentration values obtained for the different replicas were used to plot the graphs reported in the Results section.

$$\mathrm{PDI} = \left(\frac{\text{std dev.}}{\text{mean of the population}}\right)^2 \quad (4)$$

U87MG Cell Proliferation Assay. U87MG cells were seeded in a 96-well plate (3000 cells per well) and maintained in a complete medium. After 24 h, the cells were treated with sequential dilutions of 2_100K pellet or 2_16K pellet extracted from HMC3 and C20. EVs were previously suspended in sterile-filtered PBS with ions, and protein content was assessed using a Micro BCA Protein Assay Kit (ThermoFisher). EVs were diluted in the same buffer and administered to cells ranging from 0 to 500 ng of total EV protein for the 2_100K pellet, and from 0 to 31.25 ng for the 2_16K pellet. Treated cells were maintained in complete medium for 48 or 72 h, and then proliferation was quantified using CellTiter 96 Aqueous One Solution Cell Proliferation Assay (MTS, Promega) by following the supplier's instructions.

U87MG Cell Cycle Assay. U87MG cells were seeded in a 12-well plate (31,000 cells per well) and maintained in complete medium. After 24 h, cells were treated with 2.5 μg of 2_100K sample quantified with Micro BCA assay. Total cells derived from two 12-well plates with the same treatment were pooled and analyzed. Quantification of the percentage of cells in the different cell phases was performed using the Muse Cell Cycle Kit (MCH100106) using the Muse Cell Analyzer[28] by following the supplier's instructions.

U87MG Cleaved Caspase-3 Assay. U87MG cells were seeded on an 8-well chamber slide at medium−high density. The next day, cells were treated for 48 h with 25 μg/mL SEVs extracted from resting C20 cells, with the same PBS volume as

https://doi.org/10.1021/acsomega.2c00816
ACS Omega 2022, 7, 23127−23137

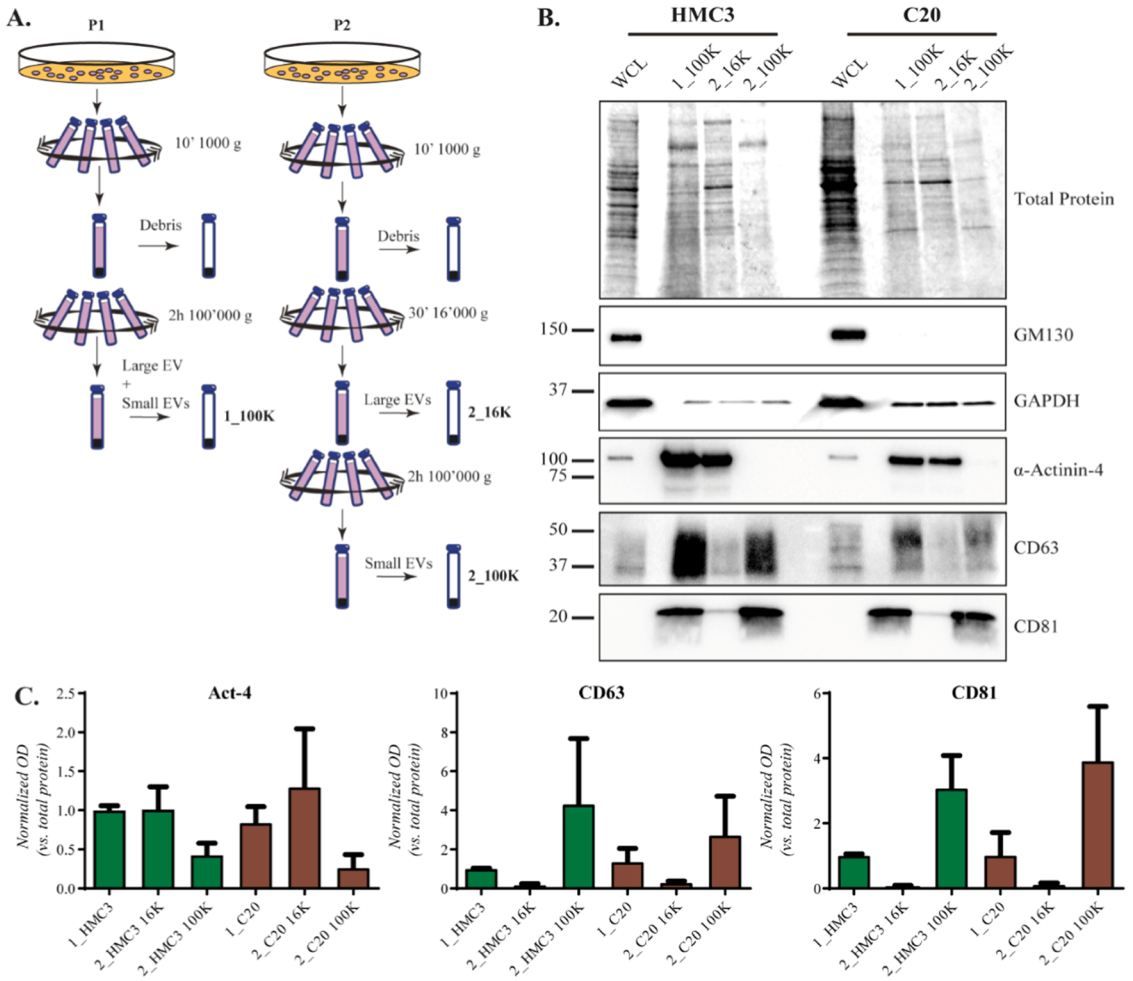

Figure 1. Panel A: Overview of both protocols (P) used in EV collection; P1 has just one step of ultracentrifugation, while P2 has an intermediate step at 16,000*g*. Panel B: EVs were gathered from HMC3 and C20 cells using P1 and P2, lysed, and the proteins separated by SDS-page. EVs gathered from one 152 cm^2 Petri dish were loaded in each lane, together with the whole-cell lysate (WCL) of each cell line. Panel C: quantification of the band intensity of WB analysis shown in panel B; the optical density (OD) was normalized on the total protein of each sample. The data represent the mean values ± SEM of at least two different experiments. The significance of the differences was determined by *t*-test vs HMC3; no significant differences were measured.

the negative control, or with 20 mM DTT for 2 h as positive apoptosis control.[29] Samples were subjected to immunofluorescence for cleaved caspase-3, as described.[30] Briefly, cells were fixed in cold 1:1 acetone:methanol solution for 15 min at −20 °C, washed three times in PBS, permeabilized with 0.5% Triton X-100 plus 2.5% BSA/PBS 5 min, blocked for 1 h at room temperature with 5% BSA/PBS, incubated overnight for an hour at 4 °C with anti-cleaved caspase-3 (1:300, 9664 Cell Signaling Technology) antibody in 2.5% BSA/PBS, and stained for 1 h at room temperature with an anti-mouseAlexa488 secondary antibody (1:100, ThermoFisher). Samples were then mounted with Fluoroshield-DAPI (Sigma-Aldrich) and imaged with a laser scanning confocal microscope (Nikon A1, Eclipse Ti), using a 20× air objective (NA 0.5) and pinhole set to 1 Airy Unit. Images were acquired at 1024 pixel × 1024 pixel resolution using a 405 nm laser (425−475 emission window) and a 488 nm laser (500−600 emission window). Cleaved caspase-3-positive cells were manually counted using ImageJ software as DAPI-positive cells displaying a mean intensity above an intensity threshold in the Alexa488 channel set according to evidently apoptotic cells in the DTT-treated sample.

miRNA Quantification (qRT-PCR). EVs pellets were suspended and lysed in Qiazol buffer (QIAGEN), total RNA was extracted using miRNeasy Micro Kit (QIAGEN, cat. 217084) by adding 5 μL of 5 nM cel-miR-39 (GenePharma) after the Qiazol step, and then following the manufacturer's protocol, extracted RNA was then quantified using NanoDrop (Thermofisher). Two hundred nanograms of total RNA was used for the reverse transcriptase reaction performed, according to the manufacturer's recommendation, using the miR-X miRNA first-strand synthesis kit (Takara) to retrotranscribe mature miRNAs. The quantification of mature miRNAs was performed with Rotor-Gene Q 2plex (Qiagen), using the SsoAdvanced SYBR Green Supermix (Bio-Rad) according to the manufacturer's protocol. The relative quantification was performed using the Rotor-Gene Q Software, by normalizing to cel-miR-39. All reactions were performed in triplicate, and the results are expressed as the mean of three biological replicates. The list of primers for the analyzed miRNA is reported in Table 1.

Gene Expression Analysis. C20 and HMC3 cells were seeded in 150 cm^2 Petri dishes and grown up to 100% confluency in complete medium. After overnight starvation, cells

https://doi.org/10.1021/acsomega.2c00816
ACS Omega 2022, 7, 23127−23137

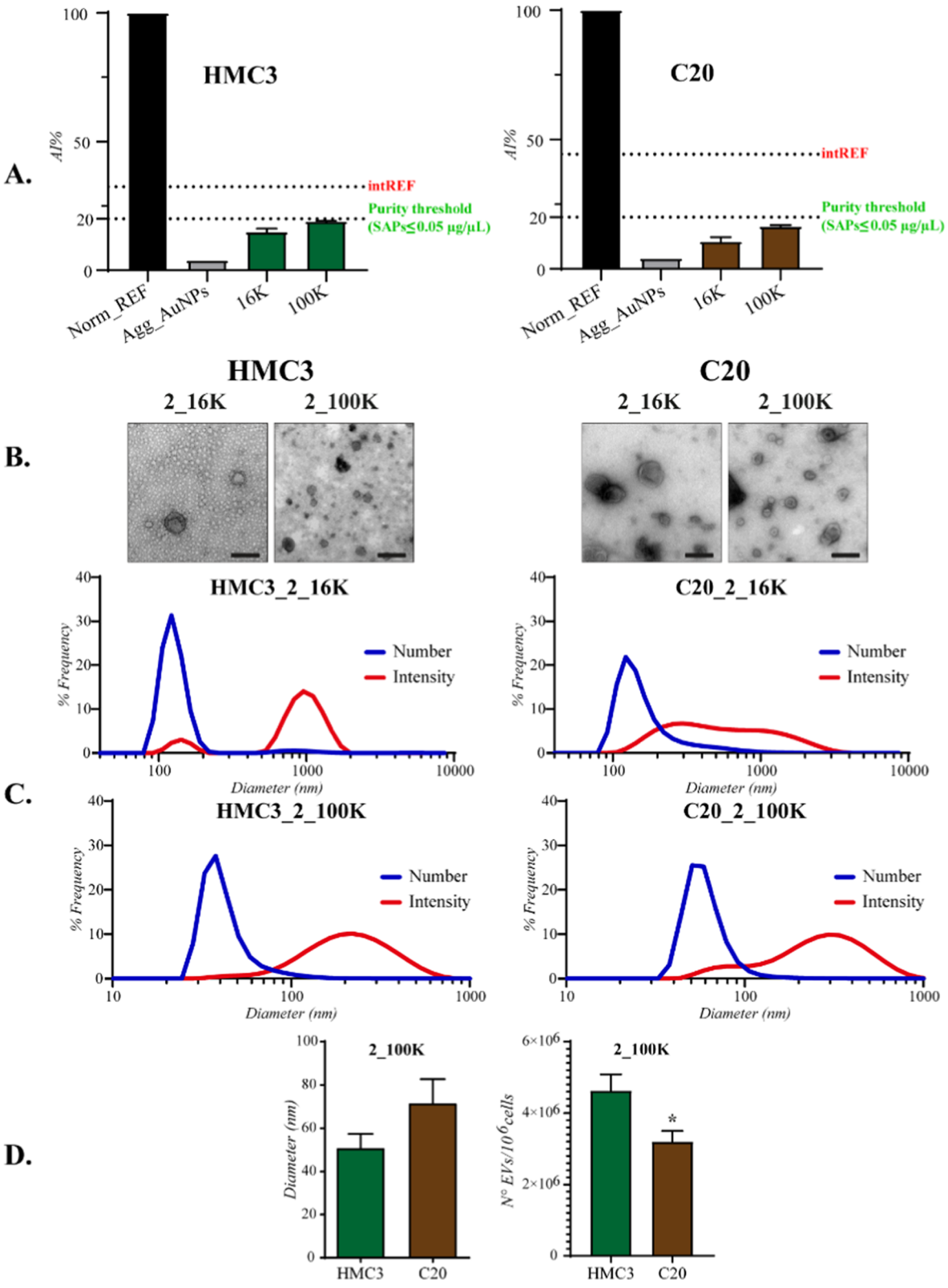

Figure 2. Biophysical analysis of EV samples gathered from HMC3 and C20 using P2. Panel A: CONAN assay-mediated purity assessment; mean AI (Aggregation Index) values of the EV preparations were normalized by the Aggregation Index of a solution of AuNPs in HPLC water (Norm_REF). A solution of HPLC water + AuNPs + PBS was used as negative control (intREF). See the main text for details. Panel B: TEM acquisitions were made with 25,000× zoom; bar indicates 100 nm. Panel C: DLS analysis; representative curves of the number and intensity values are shown for each sample gathered with P2. Panel D: DLS quantification of the 100K pellet gathered with P2 of each cell line; the number of EVs/uL was normalized by the number of cells from which EVs are derived to calculate the number of EVs secreted per million of cells. The data represent the mean values ± SEM of at least two different experiments. The significance of the differences was determined by *t*-test, $*P \leq 0.05$ vs HMC3.

https://doi.org/10.1021/acsomega.2c00816
ACS Omega 2022, 7, 23127−23137

were collected and total RNA was extracted using the Rneasy Mini Kit (Qiagen) according to the manufacturer's instructions. cDNA synthesis was performed with 1 μg of RNA using the i-Script cDNA synthesis kit (Bio-Rad) by following the manufacturer's instructions. The real-time RT-PCR reactions mix consisted of 10 μL of SsoAdvanced Universal SYBR Green Supermix (Bio-Rad), 0.5 μL of 10 μM forward and reverse primers, 5 μL of cDNA (75 ng), and 4 μL of H_2O. Reactions were performed for 40 cycles using the following temperature profile: 98 °C for 30 s; 55 °C for 30 s; and 72 °C for 3 s. The relative mRNA levels of each gene in each sample were derived from analysis of the Ct value normalized to both β-actin and GAPDH used as housekeeping genes, by using the CFX Maestro Software (Bio-Rad). The list of used primers is reported in Table 1.

Statistical Analysis. The Graph-Pad Prism program (GraphPad Software Inc., San Diego, CA) was used for data analysis and graphic presentation. All data are the mean ± SEM of at least two independent experiments. Statistical analysis was performed by ordinary one-way analysis of variance (ANOVA) with Bonferroni's multiple comparisons test, or *t*-test. $P \leq 0.05$ was considered statistically significant.

RESULTS AND DISCUSSION

Derivation and Biochemical Analysis of Human Microglia EVs. Two isolation protocols (P1 and P2) were used to gather EVs from the supernatant of human microglia HMC3 and C20 cells (Figure 1A). In P1, EVs were pooled and extracted by a single ultracentrifugation step at 100,000*g* for 2 h (1_100K). In P2, EVs were extracted by two sequential steps: 30′ at 16,000*g* (2_16K) followed by 2 h at 100,000*g* (2_100K). This was performed to obtain LEVs and SEVs after the first and second steps of centrifugation, respectively.[14]

Western blot analysis on EVs extracted from the two cell lines with the two protocols was performed. Positive EV markers α-Actinin-4, CD81, and CD63 were present only in the EV pellets, which instead did not contain the negative EV marker GM130, present in Golgi-derived intracellular vesicles of the whole-cell lysates; as the cytosolic protein recovered in all EV fractions, GAPDH was investigated and detected in both large and small EVs of the two microglia cell types (Figure 1B). α-Actinin-4 showed enrichment in the 2_16K pellet with respect to the 2_100K one from both cell lines, confirming the possibility to use this marker to discriminate the 16K population from the 100K one.[14,31] As expected, P1 allows isolation of all of the EVs produced by the cells, but without differentiating the two EV populations. By contrast, P2 allows a satisfactory separation of the large and small EVs derived from each cell line. To compare the abundance of EV markers in each lane of the gel, the optical density (OD) of every band was normalized to the total protein content in each lane (Figure 1C). The normalization showed that the two cell lines contain roughly the same amount of each marker in the different samples, suggesting that their relative abundance in the respective EVs is conserved in the two cell lines.

Biophysical Characterization of Human Microglia Evs. The purity of EV preparations was checked with the CONAN assay to demonstrate that the above-described protein analysis concerns the EV content (Figure 2A) exclusively. This assay implements the competitive tendency of citrated spherical gold nanoparticles (AuNPs) to cluster on EV membranes[32] vs getting covered by an SAP corona, in combination with gold spherical nanoparticle (AuNP) plasmonics. Soluble proteins can interfere with the interaction between the lipid membrane and AuNPs. In the presence of negligible amounts of SAPs (≤0.05 μg/μL), AuNPs cluster on the EV membrane, leading to a change in AuNP nanoplasmonics and a red shift of the localized surface plasmon resonance (LSPR) absorption peak of AuNPs. The red shift is directly related to the purity grade of the EV preparation and can be quantified by UV−vis spectroscopy through the ratio between the absorbance intensity at the LSPR peak of the AuNPs and the sum of the absorbance at 650 and 850 nm, defined as the Aggregation Index (AI).[24,33] For all of the formulations, the relative AI values resulted lower than the purity threshold (20%), indicating that in each sample, the SAP content is below 0.05 μg/μL.[24] This results confirmed that all of the proteins present in the EV samples are EV-related, confirming the capability of P2 to isolate pure EVs from human microglia cells.

Next, the morphology of HMC3 and C20 P2-derived EVs was also analyzed by transmission electron microscopy (TEM), and a panel of representative EM images is shown in Figure 2B. TEM analysis confirmed for every EV extraction the presence of of round-shaped nanoparticles with the classical cup-shaped morphology.[14,34−36] The diameter of the particles visible in the 2_16K images of both cell lines is distinctively bigger than the ones present in the 2_100K sample, in line with the separation of LEVs from SEVs that is expected with this protocol.

Finally, dynamic light scattering (DLS) was used to assess the 2_16K and 2_100K EV samples (Figure 2C,D). First, we determined both the intensity-weighted and number-weighted size distributions of the particle samples; the typical obtained curves are reported in Figure 2C as $\%I_a$ and $\%N_a$, respectively. In an ideal case of a sample consisting of a single population of EVs with a narrow polydispersity index (PDI), $\%I_a$ and $\%N_a$ would be almost identical.[27] However, in our EV samples, the two distributions are markedly different, particularly in the 2_16K but also in the 2_100K samples. This difference can be understood considering that $\%I_a$, but not $\%N_a$, is approximately proportional to the sixth power of size (see Materials and Methods), and this translates to an enhanced sensitivity vs the larger EVs in % I_a distributions. Therefore, % I_a distributions allow us to appreciate the presence of bigger EVs, even if they are present in traces. This suggests that both microglia LEVs and SEVs are heterogeneous populations of EVs comprising a wide range of possible diameters. On the other hand, $\%N_a$ values are simple particle count distributions (see Materials and Methods) and allowed to identify a prevalent peak, whose value was used to get the average diameter of the 2_100K samples (Figure 2D). The mean diameter ± SEM was 50.77 ± 20.76 nm for HMC3 and 71.48 ± 43.25 nm for C20 cells. Although this difference is not statistically significant, C20 SEVs seem to be larger and more polydispersed than HMC3 ones, as also suggested by the wider $\%I_a$ curve of the 2_100K C20 sample compared to the HMC3 one reported in Figure 2C. Furthermore, these data well fit with the quantification of the distribution and average diameter of 2_100K EVs analyzed from the TEM images (Figures 2B and S1). Overall, these diameter values are in agreement with those of EVs extracted from the most used murine microglia models, BV2 and N9, which fall in the range of 30−180 nm for BV2[37,38] and 100−160 nm for N9[39,40] cells; our results indicate that human microglia-derived small EVs have roughly the same size. Finally, DLS curves allowed estimating the number of particles present in each sample, which was normalized to the number of producing cells (Figure 2D). This analysis revealed that HMC3

https://doi.org/10.1021/acsomega.2c00816
ACS Omega 2022, 7, 23127−23137

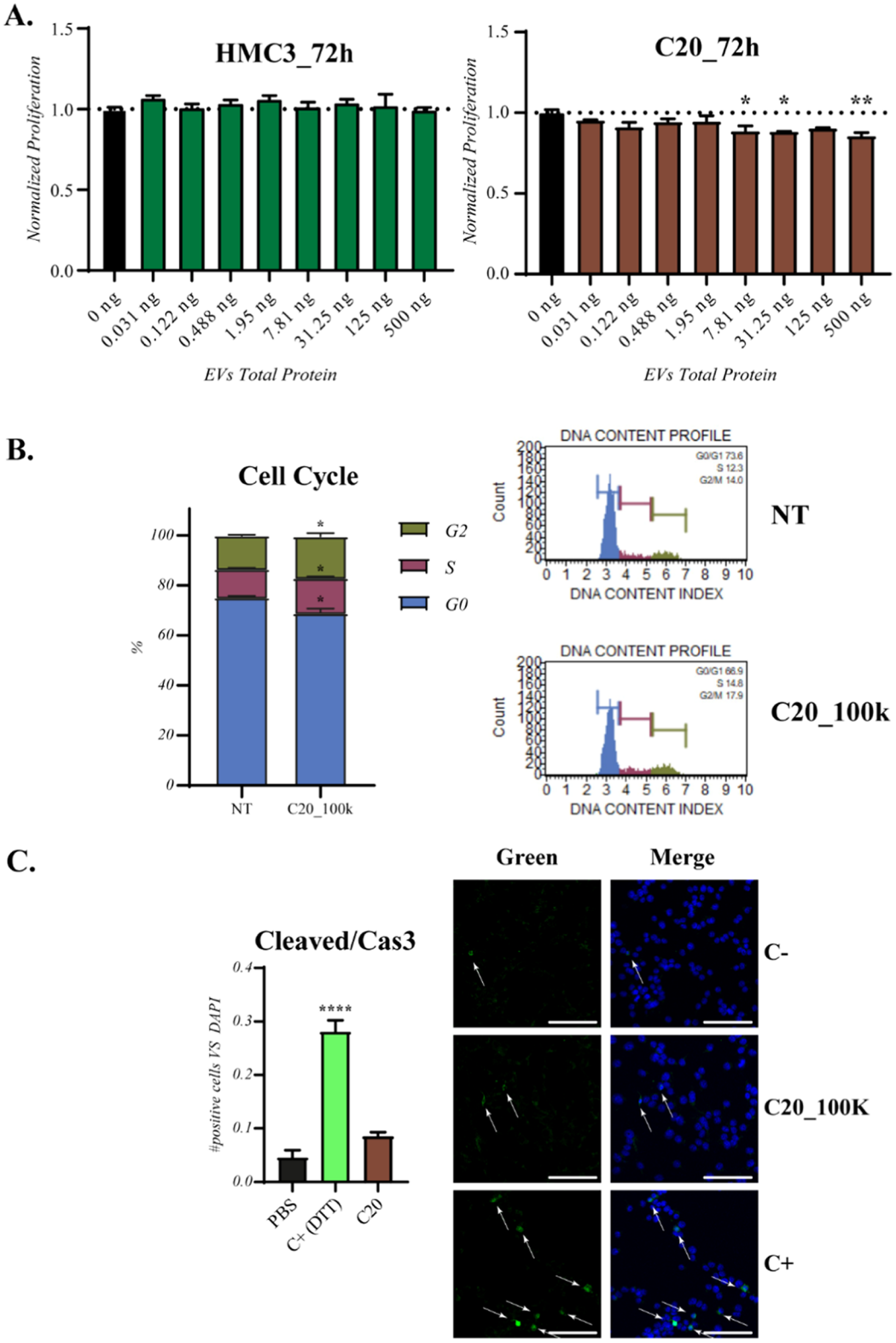

Figure 3. Panel A: proliferation assay of U87MG cells after administration of increasing concentrations of 2_100K EVs from HMC3 and C20. The administration was carried on for 72 h. The data were normalized to the control set to 1 and represent the mean values ± SEM of at least two independent experiments. The significance of the differences was determined by one-way ANOVA, followed by Bonferroni's post-test: $*P \leq 0.05$, $**P < 0.01$ vs control. Panel B: cell cycle analysis of U87MG cells treated with 100K pellet of C20 gathered with P2. The significance of the differences was determined by *t*-test: $*P \leq 0.05$, vs the respective phase of the control. Data were collected from two independent experiments. Panel C: quantification of Cleaved/Cas3 positive U87MG cells treated with PBS (C−), 100K pellet of C20 gathered with P2, and 20 mM DTT (C+). Data were quantified by counting the cell number ($n = 1929$, $n = 2183$, $n = 1694$ for C−, SEV and C+, respectively) in different analyzed fields ($n = 7$, $n = 12$, $n = 12$ for C−, SEV and C+, respectively) from two independent experiments. The significance of the differences was determined by one-way ANOVA, followed by Bonferroni's post-test: $****P \leq 0.0001$ vs the negative control.

https://doi.org/10.1021/acsomega.2c00816
ACS Omega 2022, 7, 23127−23137

cells secrete a higher number ($4.62 \times 10^6 \pm 0.47 \times 10^6$) of SEVs than C20 cells ($3.19 \times 10^6 \pm 0.31 \times 10^6$). The number of EVs per cell produced may vary based on the culture condition and extraction protocols;[41] moreover, in most cases, the concentration of EVs per mL is reported instead of the number per cell cultured. We underline that, even though the purity of the 2_16K and 2_100K EVs was comparable, the 2_16K samples contained a mixed population of EVs with highly variable diameters; this hampered a precise quantification of the mean diameter and the mean number of particles secreted, as performed for 2_100K samples.

C20-But not HMC3-Derived SEVs Can Reduce U87MG Proliferation. Once the quality of human microglia EVs was assessed, the effect of both LEVs and SEVs from the two cell lines on the proliferative capability of U87MG cells was probed. Increasing concentrations of EVs were administered, and proliferation of treated cells was measured using an MTS assay. The obtained results showed that HMC3- and C20-derived LEVs did not interfere with the proliferation capability of glioblastoma cells at any of the tested concentrations, neither after 48 nor after 72 h of treatment (Figure S2A). Similarly, HMC3- and C20-derived SEVs could not induce a change in the cell proliferation after 48 h (Figure S2B). Interestingly, only C20-derived SEVs could induce a change in the cell proliferation after 72 h of treatment, leading to a significant dose-dependent reduction of U87 proliferation, reaching an ∼15% average reduction at the highest dose tested (Figure 3A). To rule out if the observed decrease is due to a possible blockade of the cell cycle progression prompted by SEVs, or due to a direct effect on tumor cell viability, a cell cycle analysis after challenging U87MG cells with the C20-derived SEVs was first performed. As shown in Figure 3B, the SEV treatment caused a slight but significant accumulation of the cells in S and G2/M phases. Then, the presence of cleaved-caspase-3 as an apoptotic marker was also detected by immunofluorescence on the same SEV-treated C20 cells. As reported in Figure 3C, no significant induction of apoptotic phenomena was evidenced. Taken together, these data suggest that the reduction of cell proliferation prompted by C20-derived SEVs is due to their ability to interfere with the tumor cell cycle rather than viability.

Previously, other EVs produced by tumor-associated macrophages (TAM) have been demonstrated to inhibit epithelial ovarian cancer cells by suppressing metastasis and proliferation.[42,43] Moreover, it has been shown that EVs may inhibit neuroblastoma growth and immune escape upon secretion by natural killer cells.[44] Also, recently, exosomes derived from M2-polarized macrophages have been found to increase the proliferation and migration of pancreatic cancer cells.[45] However, the vast majority of studies have investigated the pro-proliferation activity of tumor-derived EVs so far, leading to the consensus that EVs can increase tumor proliferation either by acting on the tumor itself or indirectly by inhibiting immune cells.[42,46−48] In this respect, the human microglia EVs reported here showed a behavior closer to that of TAMs and immune system EVs than tumor EVs, as they do not interfere with HMC3 or even damp C20 tumor proliferation. Interestingly, a similar effect has been recently described for murine microglia BV2-derived SEVs in reducing murine glioma cell growth in vitro and in vivo.[49]

Different miRNA Signature and Polarization Status Characterize HMC3- and C20-Derived EVs. MicroRNAs (miRNA) are small noncoding RNA molecules crucially implicated in the regulation of glioma growth, and exosomes constitute one of their main delivery source to tumor cells.[50,51] This evidence prompted us to measure the abundance of eight different miRNAs (miR-21-5p, miR-26a-5p, miR-146a-5p, miR-153-3p, miR-155-5p, miR-200b-3p, miR-223-3p, and Let-7c-3p, Table 1), in HMC3- and C20-derived SEVs in order to explain the different effects on U87MG proliferation (Figure 3). The presence of miR-146a-5p, miR-155-5p, and miR-223-3p has been already identified in EVs from other microglia models;[17] some others have been found among the most analyzed miRNAs in neuroinflammation and tumor progression in the brain: miR-21-5p,[52] miR-26a-5p,[53] miR-153-3p,[54,55] miR-200b-3p,[56] and Let-7c-3p.[57] Surprisingly, the EVs of the two cell lines differed in miRNA contents. miR-26a-5p and Let-7c-3p showed a lower abundance in HMC3-derived EVs with a fold decrease with respect to the C20 of 0.50 ± 0.05 and 0.71 ± 0.21, respectively (Figure 4A). On the contrary, miR-21-5p and miR-153-3p are more abundant in HMC3 than in C20 SEVs, with a fold increase of 1.10 ± 0.06 and 1.50 ± 0.12. Remarkably, miR-146a-5p and miR-155-5p displayed a higher difference in the two samples, with an increase of 11.09 ± 1.40 for miR-146a-5p and a decrease of 0.14 ± 0.02 for miR-155-5p, in HMC3- vs C20-derived samples (Figure 4A). Based on these data, it seems unlikely that the reduction in proliferation induced by C20 SEVs (Figure 3B)

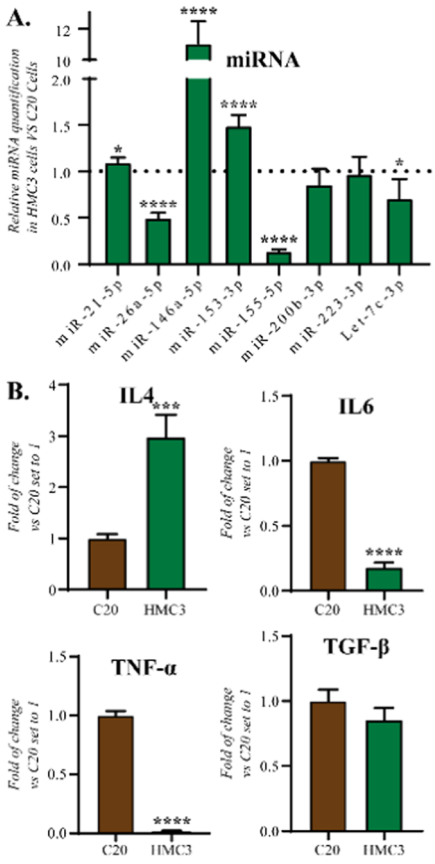

Figure 4. Panel A: Analysis of miRNA content was performed on the 2_100K EVs from both cell lines; the results were normalized on the value of the expression in the C20 cell line. Panel B: RT_PCR quantification of mRNA expression in C20 and HMC3 cells after o/n starvation. The data were expressed as the relative expression vs control set to 1 and represent the mean values ± SEM of at least two independent experiments performed in duplicate. The significance of the differences was determined by *t*-test: $^*P \leq 0.05$, $^{****}P < 0.0001$ vs the respective expression in C20, set to 1.

https://doi.org/10.1021/acsomega.2c00816
ACS Omega 2022, 7, 23127−23137

is related to the increased miR-155-5p therein, given its recognized onco-miRNA properties in the context of glioblastoma.[58] Indeed such properties may be obscured by the simultaneous variation of the other miRNA levels in the same EVs. Noteworthily, oncogenic and onco-suppressive properties have often been reported for miR-146a-5p,[59] so that the actual outcome is difficult to predict. However, another interesting possibility is that the observed miRNA changes reflect a different polarization state of the parental microglia cells, already in resting conditions. For example, miR-146a-5p and miR-155-5p have been, respectively, associated with anti-inflammatory and pro-inflammatory properties when delivered via exosomes produced by macrophages.[60] Accordingly, C20 cells could be closer to the M1 state than HMC3 cells, already in basal conditions. The production of EVs is performed in serum-free medium, which could modify per se the state of microglial cells. Thus, we selected two markers of microglia M1 sate (IL-6 and TNF-α) and two markers of M2 state (IL-4 and TGF-β)[61] and a qPCR analysis was performed on starved cells (Figure 4B). As evidenced by the results, HMC3 showed a significant increase of IL-4 gene expression and a significant decrease of TNF-α and IL-6. These data support a different polarization state of HMC3 (closer to M2) and C20 (closer to M1) donor cells, in the starvation conditions necessary for the EV collection. The M1 but not the M2 state of TAMs has been recognized as detrimental for tumor growth,[62] which could explain the observed reduction in U87MG proliferation. Finally, given the differential expression of miRNA during brain development,[17] it is also likely that these differences are related to the different developmental stages of the cells from which HMC3 and C20 cell lines were generated.

CONCLUSIONS

This paper presents a workflow for the extraction and characterization of EVs from two human microglia cell lines, C20 and HMC3 cells. Our data fill a gap in the community of microglia EVs, in which preparations from human cells have been so far poorly reported. We provided evidence that, despite most morphological, biochemical, and biophysical features being similar in the EVs from the two microglial cell types, there is a substantial difference in their miRNA cargo, already in resting conditions. In line with this observation, the two EV preparations performed differently in a biological assay. Previously, other studies confirmed that a different derivation of the same cell type can significantly affect the cargo of the secreted EVs.[63] This is possibly even more true for microglia EVs, given the highly dynamic nature of the parental cells.[11] In conclusion, despite our observations being currently limited to the analysis of eight representative miRNAs, our work could open the way to a more comprehensive study revealing even more interesting differences related to specific biological functions.

ASSOCIATED CONTENT

Supporting Information

The Supporting Information is available free of charge at https://pubs.acs.org/doi/10.1021/acsomega.2c00816.

Panel A: schematics of quantification analysis of TEM images, perimeters (yellow lines) were measured and used to calculate the diameter of each visible EVs, images were acquired at 25,000× zoom, scale bar indicates 100 nm. Panel B: quantification of the TEM images of 100K pellet gathered with P2 of each cell line. Panel C: relative frequencies distribution of the 100K pellet gathered with P2 of each cell line. The data represent the mean values ± SEM of at least two different experiments. The significance of the differences was determined by *t*-test, no significant difference between both cell line was measured (Figure S1); Panel A: proliferation assay of U87MG cells after administration of increasing concentration of 2_16K EVs from HMC3 and C20. The administration was carried on for 48 and 72 h. Panel B: proliferation assay of U87MG cells after administration of increasing concentration of 2_100K EVs from HMC3 and C20. The administration was carried on for 48 h. The data were expressed as the percentage of expression vs control set to 1 and represent the mean values ± SEM of at least two independent experiments. The significance of the differences was determined by one-way ANOVA, followed by Bonferroni's post test: no significant differences were measured (Figure S2) (PDF)

AUTHOR INFORMATION

Corresponding Authors

Laura Marchetti − *Department of Pharmacy, University of Pisa, Pisa 56126, Italy;* orcid.org/0000-0002-2110-9481; Email: laura.marchetti@unipi.it

Chiara Giacomelli − *Department of Pharmacy, University of Pisa, Pisa 56126, Italy*; Email: chiara.giacomelli@unipi.it

Authors

Lorenzo Ceccarelli − *Department of Pharmacy, University of Pisa, Pisa 56126, Italy; Department of Biotechnology, Chemistry and Pharmacy, University of Siena, 53100 Siena, Italy*

Milena Rizzo − *Institute of Clinical Physiology (IFC), CNR, Pisa 56124, Italy*

Aldo Moscardini − *SNS (Scuola Normale Superiore, NEST laboratories), Pisa 56127, Italy*

Valentina Cappello − *Center for Materials Interfaces, Electron Crystallography, Istituto Italiano di Tecnologia, Pontedera 56025, Italy*

Eleonora Da Pozzo − *Department of Pharmacy, University of Pisa, Pisa 56126, Italy;* orcid.org/0000-0003-4762-8949

Miriam Romano − *Department of Molecular and Translational Medicine, University of Brescia, Brescia 25121, Italy; Center for Colloid and Surface Science (CSGI), Firenze 50019, Italy*

Paolo Bergese − *Department of Molecular and Translational Medicine, University of Brescia, Brescia 25121, Italy; Center for Colloid and Surface Science (CSGI), Firenze 50019, Italy; Institute for Research and Biomedical Innovation- IRIB, Consiglio Nazionale delle Ricerche—CNR, Palermo 900146, Italy;* orcid.org/0000-0002-4652-2168

Claudia Martini − *Department of Pharmacy, University of Pisa, Pisa 56126, Italy;* orcid.org/0000-0001-9379-3027

Complete contact information is available at: https://pubs.acs.org/10.1021/acsomega.2c00816

Author Contributions

The manuscript was written through the contributions of all authors. All authors have given approval to the final version of the manuscript.

https://doi.org/10.1021/acsomega.2c00816
ACS Omega 2022, 7, 23127−23137

Funding

This research was funded by the institutional funds of the University of Pisa.

Notes

The authors declare no competing financial interest.

REFERENCES

(1) Paolicelli, R. C.; Bergamini, G.; Rajendran, L. Cell-to-Cell Communication by Extracellular Vesicles: Focus on Microglia. *Neuroscience* **2019**, *405*, 148−157.
(2) Potolicchio, I.; Carven, G. J.; Xu, X.; Stipp, C.; Riese, R. J.; Stern, L. J.; Santambrogio, L. Proteomic Analysis of Microglia-Derived Exosomes: Metabolic Role of the Aminopeptidase CD13 in Neuropeptide Catabolism. *J. Immunol.* **2005**, *175*, 2237−2243.
(3) Sierra, A.; Paolicelli, R. C.; Kettenmann, H. Cien Años de Microglía: Milestones in a Century of Microglial Research. *Trends Neurosci.* **2019**, 778−792.
(4) Prinz, M.; Jung, S.; Priller, J. Microglia Biology: One Century of Evolving Concepts. *Cell* **2019**, *179*, 292−311.
(5) Graeber, M. B.; Li, W.; Rodriguez, M. L. Role of Microglia in CNS Inflammation. *FEBS Lett.* **2011**, 3798−3805.
(6) Wang, W. Y.; Tan, M. S.; Yu, J. T.; Tan, L. Role of Pro-Inflammatory Cytokines Released from Microglia in Alzheimer's Disease. *Ann. Transl. Med.* **2015**, *3*, No. 136.
(7) Hong, S.; Beja-Glasser, V. F.; Nfonoyim, B. M.; Frouin, A.; Li, S.; Ramakrishnan, S.; Merry, K. M.; Shi, Q.; Rosenthal, A.; Barres, B. A.; et al. Complement and Microglia Mediate Early Synapse Loss in Alzheimer Mouse Models. *Science* **2016**, *352*, 712−716.
(8) Salter, M. W.; Stevens, B. Microglia Emerge as Central Players in Brain Disease. *Nat. Med.* **2017**, 1018−1027.
(9) Bachiller, S.; Jiménez-Ferrer, I.; Paulus, A.; Yang, Y.; Swanberg, M.; Deierborg, T.; Boza-Serrano, A. Microglia in Neurological Diseases: A Road Map to Brain-Disease Dependent-Inflammatory Response. *Front. Cell. Neurosci.* **2018**, No. 488.
(10) Geribaldi-Doldán, N.; Fernández-Ponce, C.; Quiroz, R. N.; Sánchez-Gomar, I.; Escorcia, L. G.; Velásquez, E. P.; Quiroz, E. N. The Role of Microglia in Glioblastoma. *Front. Oncol.* **2021**, *10*, No. 603495.
(11) Ceccarelli, L.; Marchetti, L.; Giacomelli, C.; Martini, C. Advances in Microglia Cellular Models: Focus on Extracellular Vesicle Production. *Biochem. Soc. Trans.* **2021**, *49*, 1791−1802.
(12) Busatto, S.; Zendrini, A.; Radeghieri, A.; Paolini, L.; Romano, M.; Presta, M.; Bergese, P. The Nanostructured Secretome. *Biomater. Sci.* **2020**, *8*, 39−63.
(13) Colombo, M.; Raposo, G.; Théry, C. Biogenesis, Secretion, and Intercellular Interactions of Exosomes and Other Extracellular Vesicles. *Annu. Rev. Cell Dev. Biol.* **2014**, *30*, 255−289.
(14) Théry, C.; Witwer, K. W.; Aikawa, E.; Alcaraz, M. J.; Anderson, J. D.; Andriantsitohaina, R.; Antoniou, A.; Arab, T.; Archer, F.; Atkin-Smith, G. K.; et al. Minimal Information for Studies of Extracellular Vesicles 2018 (MISEV2018): A Position Statement of the International Society for Extracellular Vesicles and Update of the MISEV2014 Guidelines. *J. Extracell. Vesicles* **2018**, *7*, No. 1535750.
(15) Bernimoulin, M.; Waters, E. K.; Foy, M.; Steele, B. M.; Sullivan, M.; Falet, H.; Walsh, M. T.; Barteneva, N.; Geng, J. G.; Hartwig, J. H.; et al. Differential Stimulation of Monocytic Cells Results in Distinct Populations of Microparticles. *J. Thromb. Haemostasis* **2009**, *7*, 1019−1028.
(16) Turola, E.; Furlan, R.; Bianco, F.; Matteoli, M.; Verderio, C. Microglial Microvesicle Secretion and Intercellular Signaling. *Front. Physiol.* **2012**, No. 149.
(17) Ceccarelli, L.; Giacomelli, C.; Marchetti, L.; Martini, C. Microglia Extracellular Vesicles: Focus on Molecular Composition and Biological Function. *Biochem. Soc. Trans.* **2021**, *49*, 1779−1790.
(18) Janabi, N.; Peudenier, S.; Héron, B.; Ng, K. H.; Tardieu, M. Establishment of Human Microglial Cell Lines after Transfection of Primary Cultures of Embryonic Microglial Cells with the SV40 Large T Antigen. *Neurosci. Lett.* **1995**, *195*, 105−108.
(19) Garcia-Mesa, Y.; Jay, T. R.; Checkley, M. A.; Luttge, B.; Dobrowolski, C.; Valadkhan, S.; Landreth, G. E.; Karn, J.; Alvarez-Carbonell, D. Immortalization of Primary Microglia: A New Platform to Study HIV Regulation in the Central Nervous System. *J. NeuroVirol.* **2017**, *23*, 47−66.
(20) Cohn, W.; Melnik, M.; Huang, C.; Teter, B.; Chandra, S.; Zhu, C.; McIntire, L. B.; John, V.; Gylys, K. H.; Bilousova, T. Multi-Omics Analysis of Microglial Extracellular Vesicles From Human Alzheimer's Disease Brain Tissue Reveals Disease-Associated Signatures. *Front. Pharmacol.* **2021**, *12*, No. 3078.
(21) Bohlen, C. J.; Bennett, F. C.; Tucker, A. F.; Collins, H. Y.; Mulinyawe, S. B.; Barres, B. A. Diverse Requirements for Microglial Survival, Specification, and Function Revealed by Defined-Medium Cultures. *Neuron* **2017**, *94*, 759−773.e8.
(22) Verderio, C.; Muzio, L.; Turola, E.; Bergami, A.; Novellino, L.; Ruffini, F.; Riganti, L.; Corradini, I.; Francolini, M.; Garzetti, L.; et al. Myeloid Microvesicles Are a Marker and Therapeutic Target for Neuroinflammation. *Ann. Neurol.* **2012**, *72*, 610−624.
(23) Lowry, O. H.; Rosebrough, N. J.; Farr, A. L.; Randall, R. J. Protein Measurement with the Folin Phenol Reagent. *J. Biol. Chem.* **1951**, *193*, 265−275.
(24) Zendrini, A.; Paolini, L.; Busatto, S.; Radeghieri, A.; Romano, M.; Wauben, M. H. M.; van Herwijnen, M. J. C.; Nejsum, P.; Borup, A.; Ridolfi, A.; et al. Augmented COlorimetric NANoplasmonic (CONAN) Method for Grading Purity and Determine Concentration of EV Microliter Volume Solutions. *Front. Bioeng. Biotechnol.* **2020**, *7*, No. 452.
(25) Anastasi, F.; Greco, F.; Dilillo, M.; Vannini, E.; Cappello, V.; Baroncelli, L.; Costa, M.; Gemmi, M.; Caleo, M.; McDonnell, L. A. Proteomics Analysis of Serum Small Extracellular Vesicles for the Longitudinal Study of a Glioblastoma Multiforme Mouse Model. *Sci. Rep.* **2020**, *10*, No. 20498.
(26) Moscardini, A.; Di Pietro, S.; Signore, G.; Parlanti, P.; Santi, M.; Gemmi, M.; Cappello, V. Uranium-Free X Solution: A New Generation Contrast Agent for Biological Samples Ultrastructure. *Sci. Rep.* **2020**, *10*, No. 11540.
(27) Stetefeld, J.; McKenna, S. A.; Patel, T. R. Dynamic Light Scattering: A Practical Guide and Applications in Biomedical Sciences. *Biophys. Rev.* **2016**, 409−427.
(28) Giacomelli, C.; Natali, L.; Trincavelli, M. L.; Daniele, S.; Bertoli, A.; Flamini, G.; Braca, A.; Martini, C. New Insights into the Anticancer Activity of Carnosol: P53 Reactivation in the U87MG Human Glioblastoma Cell Line. *Int. J. Biochem. Cell Biol.* **2016**, *74*, 95−108.
(29) Xiang, J.; Wan, C.; Guo, R.; Guo, D. Is Hydrogen Peroxide a Suitable Apoptosis Inducer for All Cell Types? *BioMed Res. Int.* **2016**, *2016*, 1−6.
(30) Marchetti, L.; Bonsignore, F.; Gobbo, F.; Amodeo, R.; Calvello, M.; Jacob, A.; Signore, G.; Spagnolo, C. S.; Porciani, D.; Mainardi, M.; et al. Fast-Diffusing P75NTR Monomers Support Apoptosis and Growth Cone Collapse by Neurotrophin Ligands. *Proc. Natl. Acad. Sci. U.S.A.* **2019**, *116*, 21563−21572.
(31) Kowal, J.; Arras, G.; Colombo, M.; Jouve, M.; Morath, J. P.; Primdal-Bengtson, B.; Dingli, F.; Loew, D.; Tkach, M.; Théry, C. Proteomic Comparison Defines Novel Markers to Characterize Heterogeneous Populations of Extracellular Vesicle Subtypes. *Proc. Natl. Acad. Sci. U.S.A.* **2016**, *113*, E968−E977.
(32) Montis, C.; Caselli, L.; Valle, F.; Zendrini, A.; Carlà, F.; Schweins, R.; Maccarini, M.; Bergese, P.; Berti, D. Shedding Light on Membrane-Templated Clustering of Gold Nanoparticles. *J. Colloid Interface Sci.* **2020**, *573*, 204−214.
(33) Maiolo, D.; Paolini, L.; Di Noto, G.; Zendrini, A.; Berti, D.; Bergese, P.; Ricotta, D. Colorimetric Nanoplasmonic Assay to Determine Purity and Titrate Extracellular Vesicles. *Anal. Chem.* **2015**, *87*, 4168−4176.
(34) Pascucci, L.; Scattini, G. Imaging Extracelluar Vesicles by Transmission Electron Microscopy: Coping with Technical Hurdles and Morphological Interpretation. *Biochim. Biophys. Acta, Gen. Subj.* **2021**, *1865*, No. 129648.

https://doi.org/10.1021/acsomega.2c00816
ACS Omega 2022, 7, 23127−23137

(35) Ramirez, M. I.; Amorim, M. G.; Gadelha, C.; Milic, I.; Welsh, J. A.; Freitas, V. M.; Nawaz, M.; Akbar, N.; Couch, Y.; Makin, L.; et al. Technical Challenges of Working with Extracellular Vesicles. *Nanoscale* **2018**, *10*, 881−906.
(36) Kalluri, R.; LeBleu, V. S. The Biology, Function, and Biomedical Applications of Exosomes. *Science* **2020**, *367*, No. eaau6977.
(37) Grimaldi, A.; Serpe, C.; Chece, G.; Nigro, V.; Sarra, A.; Ruzicka, B.; Relucenti, M.; Familiari, G.; Ruocco, G.; Pascucci, G. R.; et al. Microglia-Derived Microvesicles Affect Microglia Phenotype in Glioma. *Front. Cell. Neurosci.* **2019**, *13*, No. 41.
(38) Yang, Y.; Boza-Serrano, A.; Dunning, C. J. R.; Clausen, B. H.; Lambertsen, K. L.; Deierborg, T. Inflammation Leads to Distinct Populations of Extracellular Vesicles from Microglia. *J. Neuroinflammation* **2018**, *15*, No. 168.
(39) Cunha, C.; Gomes, C.; Vaz, A. R.; Brites, D. Exploring New Inflammatory Biomarkers and Pathways during LPS-Induced M1 Polarization. *Mediators Inflammation* **2016**, *2016*, 1−17.
(40) Vaz, A. R.; Pinto, S.; Ezequiel, C.; Cunha, C.; Carvalho, L. A.; Moreira, R.; Brites, D. Phenotypic Effects of Wild-Type and Mutant SOD1 Expression in N9 Murine Microglia at Steady State, Inflammatory and Immunomodulatory Conditions. *Front. Cell. Neurosci.* **2019**, *13*, No. 109.
(41) Hurwitz, S. N.; Conlon, M. M.; Rider, M. A.; Brownstein, N. C.; Meckes, D. G. Nanoparticle Analysis Sheds Budding Insights into Genetic Drivers of Extracellular Vesicle Biogenesis. *J. Extracell. Vesicles* **2016**, *5*, No. 31295.
(42) Han, C.; Zhang, C.; Wang, H.; Zhao, L. Exosome-Mediated Communication between Tumor Cells and Tumor-Associated Macrophages: Implications for Tumor Microenvironment. *OncoImmunology* **2021**, *10*, No. 1887552.
(43) Hu, Y.; Li, D.; Wu, A.; Qiu, X.; Di, W.; Huang, L.; Qiu, L. TWEAK-Stimulated Macrophages Inhibit Metastasis of Epithelial Ovarian Cancer via Exosomal Shuttling of MicroRNA. *Cancer Lett.* **2017**, *393*, 60−67.
(44) Neviani, P.; Wise, P. M.; Murtadha, M.; Liu, C. W.; Wu, C. H.; Jong, A. Y.; Seeger, R. C.; Fabbri, M. Natural Killer−Derived Exosomal MiR-186 Inhibits Neuroblastoma Growth and Immune Escape Mechanisms. *Cancer Res.* **2019**, *79*, 1151−1164.
(45) Liu, X.; Liu, K.; Zhou, D.; Mu, D.; Zhao, P. M2 Macrophage-Derived Exosomes Affects Proliferation and Migration of Pancreatic Cancer Cells via miR-21. *J. Biomater. Tissue Eng.* **2020**, *10*, 1318−13236.
(46) Maacha, S.; Bhat, A. A.; Jimenez, L.; Raza, A.; Haris, M.; Uddin, S.; Grivel, J. C. Extracellular Vesicles-Mediated Intercellular Communication: Roles in the Tumor Microenvironment and Anti-Cancer Drug Resistance. *Mol. Cancer* **2019**, 1−16.
(47) Xavier, C. P. R.; Caires, H. R.; Barbosa, M. A. G.; Bergantim, R.; Guimarães, J. E.; Vasconcelos, M. H. The Role of Extracellular Vesicles in the Hallmarks of Cancer and Drug Resistance. *Cells* **2020**, *9*, No. 1141.
(48) Becker, A.; Thakur, B. K.; Weiss, J. M.; Kim, H. S.; Peinado, H.; Lyden, D. Extracellular Vesicles in Cancer: Cell-to-Cell Mediators of Metastasis. *Cancer Cell* **2016**, 836−848.
(49) Serpe, C.; Monaco, L.; Relucenti, M.; Iovino, L.; Familiari, P.; Scavizzi, F.; Raspa, M.; Familiari, G.; Civiero, L.; D'Agnano, I.; et al. Microglia-Derived Small Extracellular Vesicles Reduce Glioma Growth by Modifying Tumor Cell Metabolism and Enhancing Glutamate Clearance through MiR-124. *Cells* **2021**, *10*, No. 2066.
(50) Buruiană, A.; Florian, Ş. I.; Florian, A. I.; Timiş, T. L.; Mihu, C. M.; Miclăuş, M.; Oşan, S.; Hrapşa, I.; Cataniciu, R. C.; et al. The Roles of MiRNA in Glioblastoma Tumor Cell Communication: Diplomatic and Aggressive Negotiations. *Int. J. Mol. Sci.* **2020**, *21*, No. 1950.
(51) Gourlay, J.; Morokoff, A. P.; Luwor, R. B.; Zhu, H. J.; Kaye, A. H.; Stylli, S. S. The Emergent Role of Exosomes in Glioma. *J. Clin. Neurosci.* **2017**, 13−23.
(52) Abels, E. R.; Maas, S. L. N.; Nieland, L.; Wei, Z.; Cheah, P. S.; Tai, E.; Kolsteeg, C. J.; Dusoswa, S. A.; Ting, D. T.; Hickman, S.; et al. Glioblastoma-Associated Microglia Reprogramming Is Mediated by Functional Transfer of Extracellular MiR-21. *Cell Rep.* **2019**, *28*, 3105−3119.e7.
(53) Qian, X.; Zhao, P.; Li, W.; Shi, Z. M.; Wang, L.; Xu, Q.; Wang, M.; Liu, N.; Liu, L. Z.; Jiang, B. H. MicroRNA-26a Promotes Tumor Growth and Angiogenesis in Glioma by Directly Targeting Prohibitin. *CNS Neurosci. Ther.* **2013**, *19*, 804−812.
(54) Ghasemi, A.; Fallah, S.; Ansari, M. MIR-153 as a Tumor Suppressor in Glioblastoma Multiforme Is Downregulated by DNA Methylation. *Clin. Lab.* **2016**, *62*, 573−580.
(55) Karsy, M.; Arslan, E.; Moy, F. Current Progress on Understanding MicroRNAs in Glioblastoma Multiforme. *Genes Cancer* **2012**, *3*, 3−15.
(56) Wu, J.; Cui, H.; Zhu, Z.; Wang, L. MicroRNA-200b-3p Suppresses Epithelial-Mesenchymal Transition and Inhibits Tumor Growth of Glioma through down-Regulation of ERK5. *Biochem. Biophys. Res. Commun.* **2016**, *478*, 1158−1164.
(57) Prada, I.; Gabrielli, M.; Turola, E.; Iorio, A.; D'Arrigo, G.; Parolisi, R.; De Luca, M.; Pacifici, M.; Bastoni, M.; Lombardi, M.; et al. Glia-to-Neuron Transfer of MiRNAs via Extracellular Vesicles: A New Mechanism Underlying Inflammation-Induced Synaptic Alterations. *Acta Neuropathol.* **2018**, *135*, 529−550.
(58) Thomas, L.; Florio, T.; Perez-Castro, C. Extracellular Vesicles Loaded MiRNAs as Potential Modulators Shared Between Glioblastoma, and Parkinson's and Alzheimer's Diseases. *Front. Cell. Neurosci.* **2020**, *14*, No. 590034.
(59) Cheng, W. C.; Liao, T. T.; Lin, C. C.; Yuan, L. T. E.; Lan, H. Y.; Lin, H. H.; Teng, H. W.; Chang, H. C.; Lin, C. H.; Yang, C. Y.; et al. RAB27B-Activated Secretion of Stem-like Tumor Exosomes Delivers the Biomarker MicroRNA-146a-5p, Which Promotes Tumorigenesis and Associates with an Immunosuppressive Tumor Microenvironment in Colorectal Cancer. *Int. J. Cancer.* **2019**, *145*, 2209−2224.
(60) Alexander, M.; Hu, R.; Runtsch, M. C.; Kagele, D. A.; Mosbruger, T. L.; Tolmachova, T.; Seabra, M. C.; Round, J. L.; Ward, D. M.; O'Connell, R. M. Exosome-Delivered MicroRNAs Modulate the Inflammatory Response to Endotoxin. *Nat. Commun.* **2015**, *6*, 1−16.
(61) Jurga, A. M.; Paleczna, M.; Kuter, K. Z. Overview of General and Discriminating Markers of Differential Microglia Phenotypes. *Front. Cell. Neurosci.* **2020**, *14*, 198.
(62) Sørensen, M. D.; Dahlrot, R. H.; Boldt, H. B.; Hansen, S.; Kristensen, B. W. Tumour-Associated Microglia/Macrophages Predict Poor Prognosis in High-Grade Gliomas and Correlate with an Aggressive Tumour Subtype. *Neuropathol. Appl. Neurobiol.* **2018**, *44*, 185−206.
(63) Murgoci, A. N.; Duhamel, M.; Raffo-Romero, A.; Mallah, K.; Aboulouard, S.; Lefebvre, C.; Kobeissy, F.; Fournier, I.; Zilkova, M.; Maderova, D.; et al. Location of Neonatal Microglia Drives Small Extracellular Vesicles Content and Biological Functions in Vitro. *J. Extracell. Vesicles.* **2020**, *9*, No. 1727637.

https://doi.org/10.1021/acsomega.2c00816
ACS Omega 2022, 7, 23127−23137